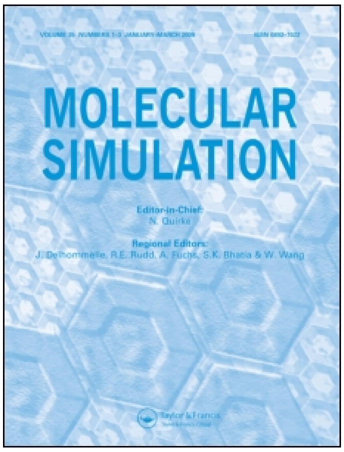

Molecular Simulation
Publication details, including instructions for authors and subscription information:
http://www.informaworld.com/smpp/title~content=t713644482

Temperature dependence of the inelastic electron tunneling

H. Nishioka[a]; T. Yamato[ab]; T. Kakitani[c]
[a] Department of Physics, Graduate School of Science, Nagoya University, Nagoya, Japan [b] CREST, Japan Science and Technology Agency, Saitama, Japan [c] Department of General Education, Faculty of Science and Technology, Meijo University, Nagoya, Japan

To cite this Article Nishioka, H. , Yamato, T. and Kakitani, T.(2006) 'Temperature dependence of the inelastic electron tunneling', Molecular Simulation, 32: 9, 727 — 734
To link to this Article: DOI: 10.1080/08927020600835665
URL: http://dx.doi.org/10.1080/08927020600835665

Molecular Simulation, Vol. 32, No. 9, 15 August 2006, 727–734

Temperature dependence of the inelastic electron tunneling

H. NISHIOKA†, T. YAMATO†‡ and T. KAKITANI¶*

†Department of Physics, Graduate School of Science, Nagoya University, Furo-cho, Chikusa-ku, Nagoya 464-8602, Japan
‡CREST, Japan Science and Technology Agency, 4-1-8 Hon-cho Kawaguchi, Saitama 332-0012, Japan
¶Department of General Education, Faculty of Science and Technology, Meijo University, Tempaku-ku, Nagoya 468-8502, Japan

(Received March 2006; in final form April 2006)

The property of the anomalous inverted region in the energy gap law which was found in the recent non-Condon theory of the electron transfer (ET) in protein media is investigated in more detail in relation to the inelastic electron tunneling. The physical aspect of the inelastic electron tunneling is theoretically discussed and schematically explained. Since it was previously shown that the inelastic electron tunneling mechanism worked significantly due to an exponential-like decay of the autocorrelation function of the electron tunneling matrix element with a small correlation time at 300 K, we investigated whether the similar exponential-like decay of the autocorrelation function is obtained or not and how the correlation time is changed at low temperatures. For this purpose, numerical calculations for the electron tunneling matrix element in the ET at 77 K from bacteriopheophytin (Bph) anion to the primary quinone in the reaction center of photosynthetic bacteria *Rhodobacter sphaeroides* are made. The results are that almost exponential-like decay of the autocorrelation function was obtained even at 77 K and the half decay time was of the similar magnitude to that at 300 K. Physical meaning of this temperature dependence is discussed.

Keywords: Non-Condon effect; Conformation fluctuation; Electron transfer; Inelastic tunneling

1. Introduction

Electron transfer (ET) in biological systems takes place by the super-exchange mechanism, enabling the long-distance ET. In such case, electronic structures of the (protein) medium play an important role. Thermal fluctuation of the medium conformation affects the electronic structure considerably, causing fluctuation of the electron tunneling matrix element T_{DA} in a delicate way [1–14]. Therefore, it is not appropriate to treat T_{DA} as constant using the Condon approximation, but the non-Condon theory is inevitable. So far, some kinds of non-Condon theories for the ET rate were published [15–21]. Among them, we recently presented a systematic non-Condon ET theory [21] which satisfies the detailed balance condition for the forward and backward ET rates. This theory has also an advantage of mathematically partitioning the ET rate into contributions from the inelastic and elastic tunneling mechanisms. The fluctuation of T_{DA} affects the ET rate through the inelastic tunneling mechanism. This non-Condon theory predicted that the Marcus inverted region [22] in the energy gap dependence of the ET rate (called the energy gap law) are remarkably modified by the inelastic tunneling mechanism; the energy gap law obtained by the non-Condon theory agrees with the Marcus parabola around the maximum ET rate region but deviates greatly to the upper value in the larger energy gap region, which we called an anomalous inverted region [21]. Based on this theoretical treatment, we discuss the physical meaning of the inelastic tunneling mechanism in some detail.

In the previous study, we showed that the autocorrelation function of $T_{DA}(t)$ at 300 K decayed by exponential forms with rather small correlation time, about 70 fs [21]. The Fourier transform of the exponential function give a Lorenz function with long tail. In such a way, the power spectrum of the autocorrelation function of $T_{DA}(t)$ had a long tail toward the large frequency. This is an origin of the inelastic tunneling and it causes the anomalous inverted region. In this respect, it is important to investigate why the autocorrelation function decays by exponential functions. To investigate its mechanism, it is useful to examine the temperature dependence of the autocorrelation function.

In this paper, we first review an essence of our non-Condon theory [21], because it becomes a guiding

*Corresponding author. Tel: + 81-52-838-2394. Fax: + 81-52-832-1170. Email: kakitani@ccmfs.meijo-u.ac.jp

Molecular Simulation
ISSN 0892-7022 print/ISSN 1029-0435 online © 2006 Taylor & Francis
http://www.tandf.co.uk/journals
DOI: 10.1080/08927020600835665

principle in the numerical analysis. Then, we calculate the autocorrelation function of the electron tunneling matrix element by a combined study of molecular dynamics (MD) simulation for the fluctuating medium at 77 K and quantum chemical calculation of T_{DA} for the ET from the bateriopheophytin anion to the primary quinone in the reaction center of the photosynthetic bacteria *Rhodobacter sphaeroides*. We compare those results with those at 300 K. Based on these results, we discuss the physical meaning of the long tail of the power spectrum.

2. Theory

We start from the Born-Oppenheimer approximation for the initial and final state of the ET reaction. We adopt the Fermi's golden rule for the ET rate, since the electronic interaction between donor and acceptor through the medium is weak. The ET rate k_{DA} is written as

$$k_{\mathrm{DA}} = \frac{2\pi}{\hbar}\left\langle \sum_{v}\left|\left\langle \Psi_{\mathrm{iu}}(\mathbf{r},\mathbf{R})|\hat{T}^{\mathrm{DA}}|\Psi_{\mathrm{fv}}(\mathbf{r},\mathbf{R})\right\rangle_{\mathbf{r},\mathbf{R}}\right|^{2} \times\delta(E_{\mathrm{iu}}-E_{\mathrm{fv}})\right\rangle_{T}, \tag{1}$$

where, the coordinates $\mathbf{r}$ and $\mathbf{R}$ are for electrons and nuclei, respectively, $\Psi_{\mathrm{iu}}(\mathbf{r},\mathbf{R})$ and $\Psi_{\mathrm{fv}}(\mathbf{r},\mathbf{R})$ are the initial and final vibronic wave functions, respectively as written as,

$$\Psi_{\mathrm{iu}}(\mathbf{r},\mathbf{R}) = \psi_i(\mathbf{r},\mathbf{R})\chi_{\mathrm{iu}}(\mathbf{R}), \tag{2}$$

$$\Psi_{\mathrm{fv}}(\mathbf{r},\mathbf{R}) = \psi_f(\mathbf{r},\mathbf{R})\chi_{\mathrm{fv}}(\mathbf{R}). \tag{3}$$

ψ_i and ψ_f are the electronic wave functions in the initial and final state, respectively, χ_{iu} and χ_{fv} are the vibrational wave functions in the initial and final state, respectively, $\hat{T}^{\mathrm{DA}}$ is the electron tunneling operator. E_{iu} and E_{fv} are the energies of the vibronic states iu and fv. The brackets $\langle\rangle_{\mathbf{r},\mathbf{R}}$ and $\langle\rangle_T$ indicate the integral over $\mathbf{r}$ and $\mathbf{R}$ and the thermal average over the initial vibrational state u at temperature T, respectively. The δ function represents that the energy is conserved for the initial vibronic state and final vibronic state namely at the time when the electron tunneling takes place.

Following the method of the group of Nitzan [23,24] and the group of Rossky [25,26], the ET rate is written in the time representation and adopt the frozen Gaussian model for the nuclear motion. Then, the ET rate k_{DA} is written as

$$k_{\mathrm{DA}} = \frac{1}{\hbar^2}\int_{-\infty}^{\infty} \mathrm{d}t\left\langle T_{\mathrm{DA}}^{\mathrm{q-c}}(t)T_{\mathrm{AD}}^{\mathrm{q-c}}(0)\right\rangle_T J(t), \tag{4}$$

where $T_{\mathrm{DA}}^{\mathrm{q-c}}(t)$ is the time-dependent quantum–classical electronic tunneling matrix element which was evaluated along the nuclear trajectory on the initial diabatic surface and is written as

$$T_{\mathrm{DA}}^{q-c}(t) = \left\langle \psi_i(\mathbf{r},\mathbf{R}(t))|\hat{T}^{\mathrm{DA}}|\psi_f(\mathbf{r},\mathbf{R}(t))\right\rangle_r, \tag{5}$$

where $\mathbf{R}(t)$ represents the center of the Gaussian wavepacket of nuclei. The quantum nature of nuclear motions is recovered when the thermal average is taken for the time correlation function, which is the origin of the notation $q-c$ in the superscript. $J(t)$ is the overlap of the two nuclear wave functions that have the same initial forms and propagate on the initial diabatic surface and the final diabatic surface, respectively. Using the frozen Gaussian model in the very short time after initiating the propagation, $J(t)$ is written as [26]

$$J(t) = \mathrm{D}(t)\exp\left[\frac{i}{\hbar}(-\Delta G-\lambda)t\right], \tag{6}$$

where $D(t)$ is the Fourier transform of the Franck-Condon factor $F(-\Delta G)$ for the ET reaction. $-\Delta G$ and λ are the energy gap and the reorganization energy for the ET reaction, respectively. In the case that only the solvent vibrations with small frequencies are considered, $F(-\Delta G)$ is written as

$$F(-\Delta G) = \frac{1}{\sqrt{4\pi\lambda k_{\mathrm{B}}T}}\exp\left[-\frac{(-\Delta G-\lambda)^2}{4\lambda k_{\mathrm{B}}T}\right]. \tag{7}$$

If the intramolecular vibrations with high frequencies are considered simultaneously, $F(-\Delta G)$ is written as

$$F(-\Delta G) = \sum_{n=0}^{\infty}\frac{\mathrm{e}^{-S}S^n}{n!}\frac{1}{\sqrt{4\pi\lambda_1 k_{\mathrm{B}}T}} \times\exp\left[-\frac{(-\Delta G-\lambda_1-n\hbar\omega S)^2}{4\lambda_1 k_{\mathrm{B}}T}\right], \tag{8}$$

where λ_1 is the reorganization energy of solvent modes and $n\hbar\omega S$ is the reorganization energy of intramolecular vibrations for the quantum number n.

We define the Fourier transform of $\langle T_{\mathrm{DA}}^{q-c}(t)T_{\mathrm{AD}}^{q-c}(0)\rangle_T$ as $P(\epsilon)$. Taking into account the quantum nature of nuclear motion by the method of Oxtoby [27], we can write $P(\epsilon)$ as follows [21]

$$P(\epsilon) = \frac{2}{1+\exp\left(-\epsilon/k_BT\right)}\frac{1}{2\pi\hbar}\int_{-\infty}^{\infty}\mathrm{d}t\langle T_{\mathrm{DA}}(t)T_{\mathrm{DA}}(0)\rangle_T \times\exp\left(\frac{i\epsilon t}{\hbar}\right), \tag{9}$$

where $\langle T_{\mathrm{DA}}(t)T_{\mathrm{DA}}(0)\rangle_T$ is the classical time-correlation function of T_{DA} with time-reversal property which is obtainable by the classical MD simulation. The $P(\epsilon)$ in equation (9) is called the power spectrum, hereafter.

The energy gap dependence of the ET rate is written as

$$k_{\mathrm{DA}}(-\Delta G) = \frac{2\pi}{\hbar}\int_{-\infty}^{\infty}\mathrm{d}\epsilon P(\epsilon)F(-\Delta G-\epsilon), \tag{10}$$

where $F(-\Delta G-\epsilon)$ is either equation (7) or (8). We define the normalized autocorrelation function $A(t)$ as

$$A(t) = \frac{\langle T_{\mathrm{DA}}(t)T_{\mathrm{DA}}(0)\rangle_T - \langle T_{\mathrm{DA}}\rangle_T^2}{\left\langle T_{\mathrm{DA}}^2\right\rangle_T - \langle T_{\mathrm{DA}}\rangle_T^2}. \tag{11}$$

Combining equation (9) with equation (11), we obtain

$$P(\epsilon) = P_{\mathrm{el}}(\epsilon) + P_{\mathrm{inel}}(\epsilon), \tag{12}$$

where

$$P_{\mathrm{el}}(\epsilon) = \left\langle T_{\mathrm{DA}}^2 \right\rangle_T \delta(\epsilon), \tag{13}$$

$$P_{\mathrm{inel}}(\epsilon) = \frac{2}{1+\exp\left(-\epsilon/k_B T\right)} \frac{\left\langle T_{\mathrm{DA}}^2 \right\rangle_T - \langle T_{\mathrm{DA}} \rangle_T^2}{2\pi\hbar} \times \int_{-\infty}^{\infty} \mathrm{d}t (A(t)-1) \exp\left(\frac{i\epsilon t}{\hbar}\right). \tag{14}$$

Since $P_{\mathrm{el}}(\epsilon)$ has an infinite value at $\epsilon = 0$, we name $P_{\mathrm{el}}(\epsilon)$ as the power spectrum for the elastic tunneling. Since $P_{\mathrm{inel}}(\epsilon)$ has an finite value for all the values of ϵ, we name $P_{\mathrm{inel}}(\epsilon)$ as the power spectrum of the inelastic tunneling.

Then, the ET rate is decoupled into two terms as follows [21]

$$k_{\mathrm{DA}}(-\Delta G) = k_{\mathrm{DA}}^{\mathrm{el}}(-\Delta G) + k_{\mathrm{DA}}^{\mathrm{inel}}(-\Delta G), \tag{15}$$

where

$$k_{\mathrm{DA}}^{\mathrm{el}}(-\Delta G) = \frac{2\pi}{\hbar} \int_{-\infty}^{\infty} \mathrm{d}\epsilon P_{\mathrm{el}}(\epsilon) F(-\Delta G - \epsilon) = \frac{2\pi}{\hbar} \left\langle T_{\mathrm{DA}}^2 \right\rangle_T F(-\Delta G), \tag{16}$$

$$k_{\mathrm{DA}}^{\mathrm{inel}}(-\Delta G) = \frac{2\pi}{\hbar} \int_{-\infty}^{\infty} \mathrm{d}\epsilon P_{\mathrm{inel}}(\epsilon) F(-\Delta G - \epsilon). \tag{17}$$

From equation (16), we find that the energy gap dependence of the ET rate due to the elastic tunneling mechanism coincides with that of the ET rate in the current theory which was obtained by the Condon approximation [22]. $k_{\mathrm{DA}}^{\mathrm{inel}}(-\Delta G)$ is the term newly produced in the ET rate expression by considering the non-Condon effect. We call this term the ET rate due to the inelastic tunneling mechanism.

3. Method

We conduct the MD simulation for the reaction center of *R. sphaeroides*. The initial configuration is obtained from the Protein Data bank, entry code 1AIJ [28]. The 262 water molecules incorporated in the structure 1AIJ were taken into account after optimization of their positions. The number of atoms used for MD is 14,631. The MD program PRESTO [29] was used with the AMBER force field [30]. We adopted a dielectric constant of 2 and approximated Coulombic potentials over 12 Å by the PPPC method [31]. The harmonic restriction was imposed on the heavy atoms in the surface residues of the protein. The same restriction was imposed on oxygen atoms of water molecules. The SHAKE algorithm [32] was used for bond stretching of hydrogen atoms. In general, on cooling the protein system to the low temperature, the protein structure is frozen into a glass state. Under such situation, protein can be trapped into different conformation depending on the protein conformation just before cooling and the manner of fluctuation in the electron tunneling current may differ among the differently trapped state. Then, many kinds of trajectories obtained starting from different protein conformation must be addressed in the analysis at low temperatures. Initially, MD simulation was conducted at 300 K. An integration time step of 1 fs was employed. After 160 ps of equilibration at 300 K, we generated a trajectory for 515 ps at 300 K. Arbitrarily we sampled 8 configurations from this trajectory. At each configuration, we cooled the system to 77 K, and conducted MD simulation of 100 ps at 77 K, confirming that the total energy is reduced to a nearly constant value within 100 ps. Then, we conducted further MD simulations of 515 ps at 77 K for the eight samples. In such a way, we obtained eight trajectories of 515 ps long starting from different configurations at 77 K. In the calculation of T_{DA} for each protein conformation, we adopted a pruned system which consists of bacteriopheophytin (Bph), primary quinone (Q_A), and the three amino acids $\mathrm{Trp}^{\mathrm{M252}}$, $\mathrm{Met}^{\mathrm{M218}}$ and $\mathrm{His}^{\mathrm{M219}}$. It was shown that these three amino acids are sufficient to substitute the role of the whole protein in the calculation of T_{DA} of the ET from Bph^- to Q_A [14]. The electronic states of the pruned protein were solved at the extended Hückel level. We referred to the FORTICON8 program [33]. We used a ITPACK 2C [34] package for solving the secular equations. To calculate electronic structures of donor and acceptor, the PM3 method [35] in the GAUSSIAN package [36] was used. The others are the same as before [21].

4. Results

We calculate the time correlation function $\langle T_{\mathrm{DA}}(t) T_{\mathrm{DA}}(0) \rangle_T$ using each trajectory. Then we calculate the autocorrelation function $A(t)$ using equation (11). Figure 1 represents time-courses of $A(t)$ for the eight trajectories at 77 K. We found that these time-courses display combinations of roughly exponential decays as a whole. From the inset of figure 1, we find that $A(t)$'s obtained by five trajectories show the similar time-courses with a half decay of $A(t)$ at 125–150 fs (solid lines), those obtained by two trajectories show the similar time-courses with a half decay of $A(t)$ at about 60 fs (dotted lines) and that obtained by one trajectory shows the time-course with a half decay of $A(t)$ at about 44 fs (dotted line). Namely, there are three types of decay of $A(t)$ among the eight trajectories. We have plotted $A(t)$ obtained by the MD simulation at 300 K [21] in the same figure (broken line). It was shown that this $A(t)$ can be expressed by the combination of three exponential functions, the largest component of which has the shortest decay time.

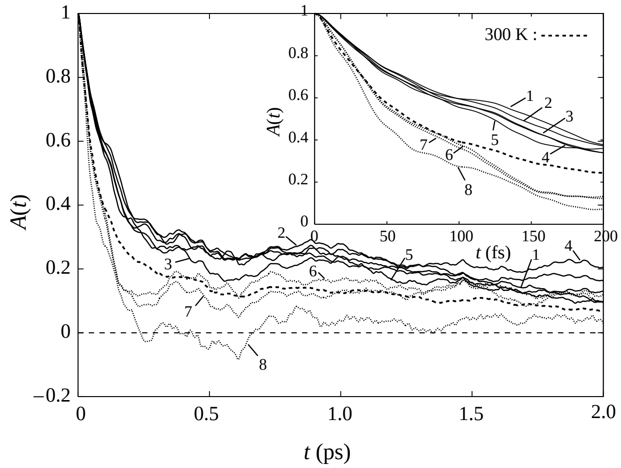

Figure 1. Plot of $A(t)$'s calculated from the 500 ps long trajectories (1, …, 8) at 77 K. $A(t)$'s for 1 – 5 (solid lines) belong to the Type I, $A(t)$'s for 6 and 7 (dotted lines) belong to the Type II, and $A(t)$'s for 8 (dotted line) belong to the Type III. For comparison, $A(t)$ calculated from the 500 ps long trajectory at 300 K is plotted by the broken line.

Therefore, two types of decay of $A(t)$ at 77 K are faster than that at 300 K while the other type of decay of $A(t)$ at 77 K is about twice slower than that at 300 K. The three types of decay of $A(t)$ would reflect the existence of three kinds of protein conformations at local energy minima, which are hardly inter-converted by the thermal fluctuation at 77 K but it can be inter-converted at 300 K. We cannot deny a possibility that there are more kind of protein conformations which may be trapped at 77 K, since we examined only eight trajectories which were obtained by the MD simulation starting from eight arbitrarily chosen conformations at 300 K.

Next, we examine whether each trajectory of 500 ps length can provide an ensemble of the local equilibrium state at 77 K. For this purpose, we divided one kind of 500 ps length trajectory (corresponding to the curve 3 in figure 1) into five trajectories with 100 ps length and calculated $A(t)$ using those short trajectories. The result is plotted in figure 2. The five decay curves of $A(t)$ fit rather well to one another until about 130 fs but disperse considerably after 130 fs. Therefore, we can say that a 500 ps trajectory does not provide an ensemble of the local equilibrium state. In consistent with this, the decay curves of $A(t)$ for the five trajectories of 500 ps of type I disperse considerably after 100 fs (curves 1 – 5 in figure 1). Judging from these simulation results, it appears that the local equilibrium state will not exist in the trapped conformations at 77 K. Since the trajectories obtained at 77 K do not correspond to ensembles of the local equilibrium state, we can only approximately obtain the power spectrum $P(\epsilon)$ at 77 K. Under such reservation, we can calculate $P_{\mathrm{inel}}(\epsilon)$ from equation (14) using $A(t)$ obtained above by the simulation calculations at 77 K. We find that a general form of $|P_{\mathrm{inel}}(\epsilon)|$ so obtained is rather similar to $P_{\mathrm{inel}}(\epsilon)$ obtained before at 300 K [21] even though the data are masked by considerable noises at large frequencies.

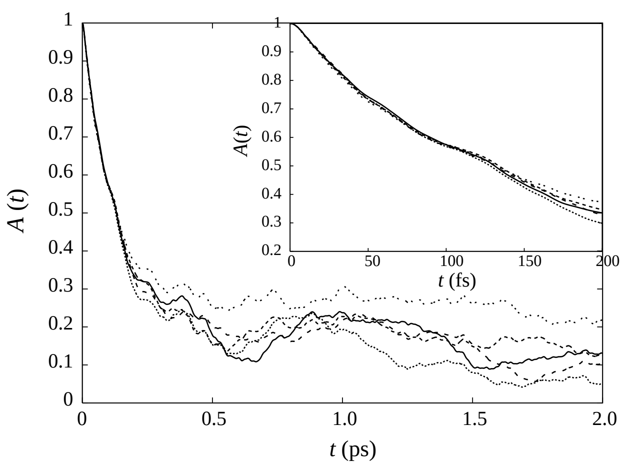

Figure 2. Plot of $A(t)$'s calculated from the 100 ps long trajectories at 77 K which are obtained by dividing the 500 ps long trajectory 3 into five pieces of trajectory.

5. Discussion

In this paper, we examined physical aspect of the inelastic electron tunneling by investigating the temperature dependence of the fluctuation of $T_{\mathrm{DA}}(t)$, and especially of the autocorrelation function $A(t)$. In the present MD simulation calculations at 77 K, we showed that $A(t)$ display some combinations of roughly exponential functions with some variation for the different trajectories. The half decay times at 77 K (44 – 150 fs) are dispersed around the half decay time at 300 K (70 fs). These results indicate that the protein conformation at 77 K is in a glass state and the fluctuations of $T_{\mathrm{DA}}(t)$ trapped at the different local potential energy minima display some variations. Except the detail, the general behavior in the decay curves of $A(t)$ at 77 K is similar to the decay curve at 300 K. Therefore, it is expected that the inelastic tunneling mechanism will work efficiently even at low temperatures.

Next, we investigate the electron tunneling route at low temperatures. In the previous study [14], we showed that $T_{\mathrm{DA}}(t)$ obtained by the MD simulation at 300 K is almost always positive when the dominant tunneling current passes through $\mathrm{Trp}^{\mathrm{M252}}$ (called Trp route), giving positive value of $\langle T_{\mathrm{DA}}\rangle_T$, while it is almost negative when the dominant tunneling current passes through $\mathrm{Met}^{\mathrm{M218}}$ (called Met route), giving negative value of $\langle T_{\mathrm{DA}}\rangle_T$. Therefore, we can investigate how much the Trp route and the Met route are used from the number of positive and negative values of $T_{\mathrm{DA}}(t)$ for each trajectory. In table 1, we list the calculated fractions of $T_{\mathrm{DA}} > 0$ and $T_{\mathrm{DA}} < 0$ and its ratio (fraction of $T_{\mathrm{DA}} > 0$/fraction of $T_{\mathrm{DA}} < 0$) for each trajectory at 77 and 300 K. From this table, we find that the fraction of $T_{\mathrm{DA}} > 0$ is much larger than the fraction of $T_{\mathrm{DA}} < 0$ at 300 K. This tendency is much more enhanced at 77 K except the trajectory 77(5). In the trajectory 77(5), the ratio is larger than that of 300 K. From these results, it appears that a special conformation is necessary to take the Met route. In most cases, the Trp route is taken at low temperatures.

Table 1. Calculated fractions of $T_{\mathrm{DA}} < 0$ and $T_{\mathrm{DA}} < 0$ and its ratio for each trajectory at 77 and 300 K. The number in the parenthesis indicates the trajectory number at 77 K. The ratio is defined as fraction of $T_{\mathrm{DA}} > 0$/fraction of $T_{\mathrm{DA}} < 0$.

Trajectory	*Fraction of $T_{DA} > 0$*	*Fraction of $T_{DA} < 0$*	*Ratio*
77(1)	0.980	0.020	49.0
77(2)	0.986	0.014	70.4
77(3)	0.992	0.008	124
77(4)	0.989	0.011	89.9
77(5)	0.678	0.322	2.1
77(6)	0.937	0.063	14.9
77(7)	0.918	0.082	11.2
77(8)	0.994	0.006	166
300	0.820	0.180	4.6

Next, we investigate the character of the fluctuation of $T_{\mathrm{DA}}(t)$. We calculate the dispersion $\sigma^2(T)$ for the fluctuation of $T_{\mathrm{DA}}(t)$ defined by

$$\sigma^2(T) = \langle T_{\mathrm{DA}}^2\rangle_T - \langle T_{\mathrm{DA}}\rangle_T^2. \tag{18}$$

In table 2, we listed the calculated dispersions and the ratio of the dispersion for each trajectory at 77 and 300 K. It should be remembered that if the fluctuation is in thermal equilibrium, the ratio should be 77/300($=0.26$). The trajectories 1–5 at 77 K which belong to the Type I have much larger values than the thermal equilibrium value of the ratio. The trajectories 6 and 7 at 77 K which belong to the Type II have the similar values to the thermal equilibrium value of the ratio. The trajectory 8 at 77 K which belongs to the Type III has considerably smaller value than the thermal equilibrium value of the ratio. Therefore, the fluctuation character is considerably different among the different conformational substates.

As expressed in equation (4), the ET rate is determined by the overlap integral between the time correlation function of the electronic tunneling matrix element $\langle T_{\mathrm{DA}}^{q-c}(t)T_{\mathrm{AD}}^{q-c}(0)\rangle_T$ and the nuclear overlap term $J(t)$ propagating on the initial and final diabatic surfaces. It should be noted that both of $\langle T_{\mathrm{DA}}^{q-c}(t)T_{\mathrm{AD}}^{q-c}(0)\rangle_T$ and $J(t)$ are complex functions of time in general. The absolute values of the two functions are decreasing functions of time. Mathematically one may argue the following [20]: If the decay time constant of $|\langle T_{\mathrm{DA}}^{q-c}(t)T_{\mathrm{AD}}^{q-c}(0)\rangle_T|$ is much larger than that of $|J(t)|$, the integral in equation (4) is mostly determined by $J(t)$, indicating that the non-Condon effect is not significant. On the other hand, if the decay time constant of $|\langle T_{\mathrm{DA}}^{q-c}(t)T_{\mathrm{AD}}^{q-c}(0)\rangle_T|$ is much smaller than that of $|J(t)|$, the integral in equation (4) is mostly determined by $\langle T_{\mathrm{DA}}^{q-c}(t)T_{\mathrm{AD}}^{q-c}(0)\rangle_T$, indicating that the non-Condon effect is significant. However, this rule does not hold when the functional forms of $|\langle T_{\mathrm{DA}}^{q-c}(t)T_{\mathrm{AD}}^{q-c}(0)\rangle_T|$ and $|J(t)|$ are not similar to one another and when the time-dependences of the phase factors of $\langle T_{\mathrm{DA}}^{q-c}(t)T_{\mathrm{AD}}^{q-c}(0)\rangle_T$ and $J(t)$ are not similar to one another. It is not easy to discuss the case when the non-Condon effect is significant and to analyze the inelastic tunneling mechanism in this time space. Instead, we discuss the above problem in the energy space. In equation (10), $k_{\mathrm{DA}}(-\Delta G)$ is expressed as an integral of the overlap between $P(\epsilon)$ and $F(-\Delta G-\epsilon)$. In the elastic tunneling process, the energy gap is modified to $-\Delta G-\epsilon$. The shifted energy ϵ comes from the fluctuation of $T_{\mathrm{DA}}(t)$, namely by means of the conformation change of the protein environment. Based on this fact, we consider that ϵ is the energy difference between the initial and final states which is related to the dynamically coupled interaction of nuclei and electrons under thermal fluctuations, in consistent with the definition of $T_{\mathrm{DA}}(t)$ in equation (5). The energy ϵ on which we focused in the power spectrum in the present study is too large to be considered as vibrational or phonon energy emitted or absorbed during the electron tunneling. It should be a mixed energy of electron and nuclear motions in the virtual process of electron tunneling inherent to the non-Condon effect. Here, one should remind of the fact that a reasonable reaction coordinate in the ET is the energy difference between the initial and final state [37]. The energy ϵ is used to reduce the energy gap (energy difference between the initial and final state) in the inelastic tunneling mechanism. In this connection, it should be remembered that the important physical quantities in the ET reaction are the reorganization energy, energy gap and reaction coordinate which work to connect the two states; initial and final states.

In the following, we schematically explain how the inelastic tunneling mechanism works in the ET rate. In figure 3, we show the free energy curves for the initial (I) and final (F) state by the solid line on the left and the power spectrum $P(\epsilon)$ on the right. These free energy curves are drawn as a typical case of the inverted region of the energy gap law. The form of the power spectrum $P(\epsilon)$ is tentatively drawn by using the data at 300 K obtained by our previous study [21]. Corresponding to a value of ϵ, the energy gap is reduced by ϵ. In figure 3, the final free energy curve is drawn (dotted line) by shifting upward by ϵ in order to represent the reduction of the energy gap by ϵ. Each value of ϵ ($\neq 0$) opens the inelastic electron tunneling channel. In the case of $\epsilon = 0$, the elastic tunneling mechanism works corresponding to the ET in the ordinary Condon theory. The transition state for each value of ϵ is marked by a circle on the initial free energy curve (represented by $1^*, \cdots, 5^*$). The activation energy $\Delta G^{\ddagger}$ for the reaction decreases in order of 5^*, 1^*, 2^*, 3^* and 4^* in figure 3. The contribution of each channel to the ET rate is given by a product of $P(\epsilon)$ and the activation

Table 2. Calculated dispersion $\sigma^2(77)$ of $T_{\mathrm{DA}}(t)$ and ratio for each trajectory at 77 K. $\sigma^2(300)$ is the dispersion at 300 K. The ratio is defined as $\sigma^2(77)/\sigma^2(300)$.

Trajectory	*Dispersion σ^2($\times 10^{-8}$ eV^2)*	*Ratio*
77(1)	2.47	0.47
77(2)	2.65	0.51
77(3)	2.16	0.41
77(4)	2.57	0.49
77(5)	1.92	0.37
77(6)	1.17	0.22
77(7)	1.24	0.24
77(8)	0.96	0.18
300	5.24	

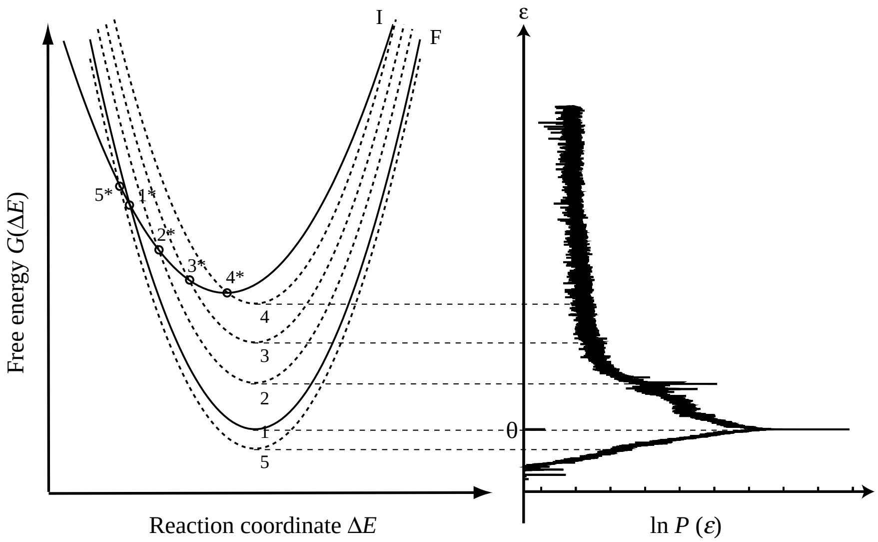

Figure 3. Plot of the free energy curves as a function of the reaction coordinate for the initial (I) and final (F) state (on the left). Plot of ln $P(\epsilon)$ calculated from the $A(t)$ obtained at 300 K (on the right). The broken curves on the left indicates the free energy curve of the final state shifted by ϵ upward. The circle represents the transition state for the reaction from the initial state to the final state shifted by ϵ.

factor $\exp(-\Delta G^{\ddagger}/k_B T)$. This activation factor is proportional to the Franck-Condon factor $F(-\Delta G - \epsilon)$ in the above discussion. $P(\epsilon)$ has a large peak at $\epsilon = 0$, decreases rapidly in the small value of $\epsilon(>0)$ and decreases slowly in the larger value of ϵ. $P(\epsilon)$ decreases much rapidly for $\epsilon < 0$. Therefore, when the activation energy is large as represented by 1$*$ in figure 3, the channel of the elastic tunneling ($\epsilon = 0$) does not work efficiently even if $P(0)$ is large but the channels through 4$\cdots$3 of the inelastic tunneling ($\epsilon > 0$) work efficiently. This non-Condon effect causes the decrease of the activation energy in the inverted region.

In our calculations, the decay time constant of $A(t)$ at 77 K is almost comparable to that at 300 K. Similar results for the ET reactions in Ru-modified arurin are reported by Skourtis *et al.* [20]. In their simulations, the correlation time of the calculated autocorrelation function of T_{DA} at 3 K is almost comparable to that at 310 K [20]. These results must suggest a significant physical implication for the electron tunneling mechanism in protein environment. Usually it is believed that the fluctuation of conformation is weaken as the temperature is lowered. Indeed, this expectation will hold true when one discusses the actual energy flow over the barrier. However, it does not apply to the electron tunneling matrix element. Even if the conformation fluctuation is weaken by lowering the temperature, the decay constant of the autocorrelation function of the electron tunneling matrix element is not significantly affected. This phenomenon will reflect the fact that the rapid change of the electron tunneling matrix element might be due to a sudden change in the combination of interatomic tunneling current J_{ab} expressed by [38–40]

$$T_{DA} = \hbar \sum_{a \in \Omega_D} \sum_{b \notin \Omega_D} J_{ab}, \tag{19}$$

where a and b are the numbering of atoms, Ω_D represents the donor region where the whole space is divided by an arbitrary plane j between donor and acceptor. The total tunneling currents passing through any plane cut between donor and acceptor is conserved by the continuity condition. In order to satisfy this continuity condition for any value of T_{DA} corresponding to different conformations, the amplitude and the phase of each J_{ab} must adjust itself all the way. As a result, each J_{ab} must change quickly and abruptly in accordance with a small change of the protein conformation. Namely, the amplitude and sign of J_{ab} is not determined by the local condition such as bond length and the bond angle nearby, but is determined by the condition of the whole protein conformation self consistently. This is done by readjusting the overall electronic wave function to conform to the new protein conformation. In such a way, the interatomic tunneling currents J_{ab} will vary almost randomly and cause the diffuse property to the decay in $A(t)$ as expressed by exponential forms. When the electronic redistribution is brought about by a minute conformation change, we shall obtain $A(t)$ which is almost independent of temperature. Our simulation results of $A(t)$ support this possibility.

As found from the above discussion, the electron tunneling matrix element is much sensitive to the protein conformation. Therefore, this property can be used to search conformational substates at low temperatures [41]. In figure 1, we found three conformational substates from eight kinds of trajectories at 77 K by plotting the autocorrelation function $A(t)$. By choosing more kinds of trajectories, we may find more conformational substates. Namely, the calculation of the autocorrelation function $A(t)$ at low temperatures can be a powerful theoretical tool for finding the hierarchy of conformational substates of protein, as probed by the electron tunneling property.

In our study, we discussed that conformation fluctuations in the time range of 10 fs play a significant role in the ET reaction by the inelastic tunneling mechanism. There may be a claim for this analysis that the uncertainty principle will not be satisfied. The splitting energy due to the electron tunneling, $2|T_{\mathrm{DA}}|$, is too small to discuss such a short time (10 fs) dynamics by the classical treatment for the nuclear motion. Indeed, using the typical value of $|T_{\mathrm{DA}}| = 10^{-4}$ eV and $\Delta t = 10$ fs, we obtain

$$|T_{\mathrm{DA}}| \cdot \Delta t = 3 \times 10^{-3}\, \hbar, \tag{20}$$

which does not satisfy the uncertainty principle $|T_{\mathrm{DA}}| \cdot \Delta t > \hbar$. Under such situation, a quantum mechanical treatment of nuclear and electron motions is inevitable. We should mention that this problem is overcome in our theory because we made quantum correction for the motion of nuclei and electrons in obtaining $P(\epsilon)$ as shown in equation (9). Namely, even if we treated the nuclear motion classically in the calculation of $T_{\mathrm{DA}}(t)$ for each protein conformation at each time, we recovered the quantum mechanical property of the nuclear and electron motion by an empirical method when we calculate $P(\epsilon)$.

6. Conclusion

In this paper, we investigated the temperature dependence of the inelastic electron tunneling property by the combined study of the MD simulations and calculations of the electron tunneling matrix element $T_{\mathrm{DA}}(t)$ by quantum chemistry. We collected 8 trajectories of $T_{\mathrm{DA}}(t)$ which were obtained by the MD simulations at 77 K started from the eight arbitrary protein conformations in the equilibrium state at 300 K. We found that the autocorrelation function $A(t)$ decayed by almost exponential functions with half decay times of 44–150 fs, depending on the trajectories. A slightly different property of $A(t)$ among the trajectories indicates that the protein conformation is in the glass state at 77 K and the protein conformation is trapped at the local energy minimum. Analyzing the property of $A(t)$ by splitting the trajectory into some parts, we found that the local equilibrium is not attained in each trajectory. The decay property of $A(t)$ at 77 K roughly agrees with that obtained at 300 K. Although the thermal equilibrium is not attained at 77 K, we can approximately calculate $P(\epsilon)$ using the above $A(t)$. We expect that the long tail in $P(\epsilon)$ should be obtained, in the similar way as 300 K. Combining these results with the fact that the width of the Franck-Condon factor as a function of the energy gap in equations (7) and (8) becomes narrower at low temperatures, we expect that the anomalous inverted region will become much easier to be observed at low temperatures. Judging from the large energy as much as 1–2 eV in the long tail of $P(\epsilon)$, its energy is not due to pure vibration or phonon, but it is due to a mixed motion of electron and nucleus inherent to the non-Condon effect. This mixed energy of electronic and nuclear motions is not observable by itself but it contributes to the electron tunneling process virtually by means of shifting the energy difference between the initial and final state. We schematically represented this virtual process to visualize the inelastic electron tunneling mechanism.

Acknowledgements

This work was supported by the Grant-in-Aid on Scientific Research to T.K. from the Ministry of Education, Culture, Sports, Science and Technology of Japan. This work was also supported by Grants-in-Aid for the 21st Century COE Program "Frontiers of Computational Science" from the Ministry of Education, Culture, Sports, Science and Technology of Japan to T.Y.

References

[1] D.N. Beratan, J.N. Onuchic, J.J. Hopfield. Electron tunneling through covalent and noncovalent pathways in proteins. *J. Chem. Phys.*, **86**, 4488 (1987).
[2] J.N. Onuchic, D.N. Beratan, J.R. Winkler, H.B. Gray. Pathway analysis of protein electron-transfer reactions. *Annu. Rev. Biophys. Biomol. Struct.*, **21**, 349 (1992).
[3] J.J. Regan, A.J. Di Bilio, R. Langen, L.K. Skov, J.R. Winkler, H.B. Gray, J.N. Onuchic. Electron tunneling in azurin: the coupling across a β-sheet. *Chem. Biol.*, **2**, 489 (1995).
[4] P.C.P. de Andrade, J.N. Onuchic. Generalized pathway model to compute and analyze tunneling matrix elements in proteins. *J. Chem. Phys.*, **108**, 4249 (1998).
[5] D.S. Wuttke, J.H. Bjerrum, J.R. Winkler, H.B. Gray. Electron-tunneling pathways in cytochrome. *c. Science*, **256**, 1007 (1992).
[6] W.B. Curry, M.D. Grabe, I.V. Kurnikov, S.S. Skourtis, D.N. Beratan, J.J. Regan, A.J.A. Aquino, P. Beroza, N.N. Onuchic, J.N Onuchic. Pathways, pathway tubes, pathway docking and propagators in electron transfer proteins. *J. Bioenerg. Biomemb.*, **27**, 285 (1995).
[7] I. Daizadeh, E.S. Medvedev, A.A. Stuchebrukhov. Effect of protein dynamics on biological electron transfer. *Proc. Natl. Acad. Sci. USA*, **94**, 3703 (1997).
[8] J. Antony, D.M. Medvedev, A.A. Stuchebrukhov. Theoretical study of electron transfer between the photolyase catalytic cofactor $FADH^-$ and DNA thymine dimer. *J. Am. Chem. Soc.*, **122**, 1057 (2000).
[9] I.A. Bababin, J.N. Onuchic. Dynamically controlled protein tunneling paths in photosynthetic reaction centers. *Science*, **290**, 114 (2000).
[10] Q. Xie, G. Archontis, S.S. Skourits. Protein electron transfer: a numerical study of tunneling through fluctuating bridges. *Chem. Phys. Lett.*, **312**, 237 (1997).
[11] T. Kawatsu, T. Kakitani, T. Yamato. Destructive interference in the electron tunneling through protein media. *J. Phys. Chem. B*, **106**, 11356 (2002).
[12] C. Kobayashi, K. Baldridge, J.N. Onuchic. Multiple versus single pathways in electron transfer in proteins: Influence of protein dynamics and hydrogen bonds. *J. Chem. Phys.*, **119**, 3550 (2003).
[13] M.-L. Tan, I.A. Balabin, J.N. Onuchic. Dynamics of electron transfer pathways in cytochrome *c* oxidase. *Biophys. J.*, **86**, 1813 (2004).
[14] H. Nishioka, A. Kimura, T. Yamato, T. Kawatsu, T. Kakitani. Interference, fluctuation, and alternation of electron tunneling in protein media. 1. Two tunneling routes in photosynthetic reaction center alternate due to thermal fluctuation of protein conformation. *J. Phys. Chem. B*, **109**, 1978 (2005).
[15] J. Tang. Effects of a fluctuating electronic coupling matrix element on electron transfer rate. *J. Chem. Phys.*, **98**, 6263 (1993).

[16] I.A. Goychuk, E.G. Petrov, V. May. Bridge-assisted electron transfer driven by dichotomically fluctuating tunneling coupling. *J. Chem. Phys.*, **103**, 4937 (1995).
[17] E.S. Medvedev, A.A. Stuchebrukhov. Inelastic tunneling in long-distance biological electron transfer reactions. *J. Chem. Phys.*, **107**, 3821 (1997).
[18] M. Bixon, J. Jortner. Effects of configurational fluctuation on electronic coupling for charge transfer dynamics. *Russ. J. Electrochem.*, **39**, 3 (2003).
[19] A. Troisi, A. Nitzan, M.A. Ratner. A rate constant expression for charge transfer through fluctuating bridges. *J. Chem. Phys.*, **119**, 5782 (2003).
[20] S.S. Skourtis, I.A. Balabin, T. Kawatsu, D.N. Beratan. Protein dynamics and electron transfer: electronic decoherence and non-Condon effects. *Proc. Natl. Acad. USA*, **102**, 3552 (2005).
[21] H. Nishioka, A. Kimura, T. Yamato, T. Kawatsu, T. Kakitani. Interference, fluctuation, and alternation of electron tunneling in protein media. 2. Non-condon theory for the energy gap dependence of electron transfer rate. *J. Phys. Chem. B*, **109**, 15621 (2005).
[22] R.A. Marcus, N. Sutin. Electron transfers in chemistry and biology. *Biochim. Biophys. Acta*, **811**, 265 (1985).
[23] E. Neria, A. Nitzan, R.N. Barnett, U. Landman. Quantum dynamical simulations of non-adiabatic processes: solvation dynamics of the hydrated electron. *Phys. Rev. Lett.*, **67**, 1011 (1991).
[24] E. Neria, A. Nitzan. Semiclassical evaluation of nonadiabatic rates in condensed phases. *J. Chem. Phys.*, **99**, 1109 (1993).
[25] B.J. Schwartz, E.R. Bittner, O.V. Prezhdo, P.J. Rossky. Quantum decoherence and the isotope effect in non-adiabatic molecular dynamics simulations. *J. Chem. Phys.*, **104**, 5942 (1996).
[26] O.V. Prezhdo, P.J. Rossky. Evaluation of quantum transition rates from quantum-classical molecular dynamics simulations. *J. Chem. Phys.*, **107**, 5863 (1997).
[27] D.W. Oxtoby. Vibrational population relaxation in liquids. *Adv. Chem. Phys.*, **47**, 487 (1981).
[28] M.H.B. Stowell, T.M. McPhillips, D.C. Rees, S.M. Soltis, E. Abresch, G. Feher. Light-induced structural changes in photosynthetic reaction center: implications for mechanism of electron–proton transfer. *Science.*, **276**, 812 (1997).
[29] K. Morikami, T. Nakai, A. Kidera, M. Saito, H. Nakamura. PRESTO: a vectorized molecular mechanics program for biopolymers. *Comput. Chem.*, **16**, 243 (1992).
[30] W.D. Cornell, P. Cieplak, C.I. Bayly, I.R. Gould, K.M. Merz, D.M. Ferguson, D.C. Spellmeyer, T. Fox, J.W. Caldwell, P.A. Kollman. A second generation force field for the simulation of proteins, nucleic acids, and organic molecules. *J. Am. Chem. Soc.*, **117**, 5179 (1995).
[31] M. Saito. Molecular dynamics simulations of proteins in water without the truncation of long-range Coulomb interactions. *Mol. Simul.*, **8**, 321 (1992).
[32] J.P. Ryckaert, G. Ciccotti, H.J.C. Berendsen. Numerical integration of the Cartesian equations of motion of a system with constraints: molecular dynamics of *n*-alkanes. *J. Comp. Phys.*, **23**, 327 (1977).
[33] J. Howell, A. Rossi, D. Wallace, K. Haraki, R. Hoffmann. FORTICON8 (extended Hückel method program). *QCPE*, **11**, 344 (1977).
[34] D.R. Kincaid, J.R. Respess, D.M. Young, R.G. Grimes. *ITPACK 2C*; University of Texas: Austin, TX (1999) (a fortran package for solving large sparse linear system by adaptive accelerated iterative methods).
[35] J.J.P. Stewart. Optimization of parameters for semiempirical methods I. Method. *J. Comp. Chem.*, **10**, 209 (1989).
[36] M.J. Frisch, G.W. Trucks, H.B. Schlegel, G.E. Scuseria, M.A. Robb, J.R. Cheeseman, V.G. Zakrzewski, J.A. Montgomery, R.E. Stratmann, J.C. Burant, S. Dapprich, J.M. Millam, A.D. Daniels, K.N. Kudin, M.C. Strain, O. Farkas, J. Tomasi, V. Barone, M. Cossi, R. Cammi, B Mennucci, C Pomelli, C Adamo, S Clifford, J Ochterski, G.A Petersson, P.Y Ayala, Q Cui, K Morokuma, D.K Malick, A.D Rabuck, K Raghavachari, J.B Foresman, J Cioslowski, J.V Ortiz, A.G Baboul, B.B Stefanov, G Liu, A Liasheko, P Piskorz, I Komaromi, R Gomperts, R.L Martin, D.J Fox, T Keith, M.A Al-Laham, C.Y Peng, A Nanayakkara, M Challacombe, P.M.W Gill, B Johnson, W Chen, M.W Wong, J.L Andres, C Gonzalez, M Head-Gordon, E.S Replogle, J.A Pople. *Gaussian98*, revisionA.9; Gaussian, Inc., Pittsburgh PA (1998).
[37] A. Yoshimori, T. Kakitani, Y. Enomoto, N. Mataga. Shapes of the electron-transfer rate vs energy gap relations in polar solutions. *J. Phys. Chem.*, **93**, 8316 (1989).
[38] A.A. Stuchebrukhov. Tunneling currents in electron transfer reaction in proteins. II. Calculation of electronic superexchange matrix element and tunneling currents using nonorthogonal basis sets. *J. Chem. Phys.*, **105**, 10819 (1996).
[39] T. Kawatsu, T. Kakitani, T. Yamato. A novel method for determining the electron tunneling pathway in protein. *Inorg. Chim. Acta*, **300–302**, 862 (2000).
[40] T. Kawatsu, T. Kakitani, T. Yamato. Worm model for electron tunneling in proteins: consolidation of the pathway model and the Dutton plot. *J. Phys. Chem. B*, **105**, 4424 (2001).
[41] H. Frauenfelder, F. Parak, R.D. Young. Conformational substates in proteins. *Annu. Rev. Biophys. Biophys. Chem.*, **17**, 451 (1988).